Journal of Membrane Science 641 (2022) 119872

Contents lists available at ScienceDirect

Journal of Membrane Science

journal homepage: www.elsevier.com/locate/memsci

Salt storage and induced crystallisation in porous asymmetric inorganic membranes

Weng Fu [a,b], Julius Motuzas [a], David Wang [a,c], Christelle Yacou [a,d], Anne Julbe [e], James Vaughan [b,*], João C. Diniz da Costa [a,f,g]

[a] The University of Queensland, FIM²Lab – Functional Inorganic Materials and Membrane Laboratory, School of Chemical Engineering, Brisbane, Qld, 4072, Australia
[b] The University of Queensland, Hydrometallurgy Research Group, School of Chemical Engineering, Brisbane, Qld, 4072, Australia
[c] The University of Sydney, School of Chemical and Biomolecular Engineering, Sydney, NSW, 2006, Australia
[d] Université des Antilles, Laboratory COVACHIM-M2E, EA 3592, BP 250, 97157, Pointe-à-Pitre, Guadeloupe, France
[e] Institut Européen des Membranes (IEM, UMR 5635 CNRS, ENCM, UM), Université de Montpellier, CC47, Place Eugène Bataillon, 34095, Montpellier Cedex 5, France
[f] LAQV-REQUIMTE, (Bio)Chemical Process Engineering, Department of Chemistry, Faculty of Science and Technology, Universidade NOVA de Lisboa, 2829-516, Caparica, Portugal
[g] iBET – Instituto de Biologia Experimental e Tecnológica, 2781-901, Oeiras, Portugal

ARTICLE INFO

Keywords:
Inorganic membranes
Pore storage
Pore size control
Pervaporation
Crystallisation

ABSTRACT

Processing brines to recover strategic mineral salts using evaporation ponds requires large surface areas and are slow, even in arid climates. Here we show a novel membrane macropore storage mechanism that induces fast salt crystallisation in mesoporous top-layers in inorganic asymmetric membranes, stemming from 789 million nucleation points per metre square of surface area. During membrane pervaporation, dissolved salts are retained mainly in the macropores of the substrate which subsequently provide ideal conditions for crystal nucleation and growth on the membrane surface upon drying. This novel pore storage mechanism is attained owing to the solution flow modulation of the mesoporous titania and gamma-alumina layers that is counterbalanced by the flow of water during pervaporation. Therefore, pore size control is imperative to avoid flooding in the macroporous substrate. This work further shows the fundamental properties of the salt storage mechanism described by a single salt production coefficient, and a global salt production coefficient for metal chloride salts. This technology could potentially be considered for unlocking and process strategic global minerals from brines.

1. Introduction

The demand for strategic minerals to meet our contemporary societies need for technological advancement is expanding. Meanwhile, conventional orebody grades are in decline, thus mineral brine mines will be an increasingly important source of salts and metals in the future. A clear example is lithium, a relatively rare metal required for the production of highly efficient batteries for portable electronic devices [1], plug-in electrical cars [2] and increasingly for large scale power storage [3]. The estimated global lithium brine reserves of 21.6 Mt is 5.6 times larger than non-brine lithium reserves [4]. Even larger reserves are the oceans of the world which are last frontier in mineral processing, holding vast quantities of dissolved metal ions of commercial interest, such as lithium ($2.3x10^5$ Mt), nickel (8,600 Mt), magnesium ($1.3x10^{12}$ Mt), gold (14.5 Mt), potassium ($5.1x10^8$ Mt), manganese (500 Mt) and uranium (4,300 Mt) among many others [5]. These elements find broad application in wealth generation (gold), and advanced materials such as magnesium for medical applications [6], manganese doped semiconductor quantum dots [7] and nickel as catalyst [8]. In addition, potassium plays a critical role in food production [9] and uranium is a key element to nuclear power production in a decarbonised economy [10]. However, extracting valuable elements from mineral brines is time and energy intensive and expensive, particularly in the case of diluted metal ions in oceans [11].

Mineral brines are traditionally processed in evaporation ponds and industrial crystallisers. Essentially these processes evaporate water from a brine solution, leading to supersaturation and crystallisation. The crystallisation of evaporation ponds is very slow and highly dependable upon the weather conditions whilst industrial crystallisers deliver fast crystallisation rates though are energy intensive. Since the 1980s,

* Corresponding author.
E-mail address: james.vaughan@uq.edu.au (J. Vaughan).

https://doi.org/10.1016/j.memsci.2021.119872
Received 24 July 2021; Received in revised form 1 September 2021; Accepted 13 September 2021
Available online 21 September 2021

polymeric hydrophobic membranes have become attractive to promote crystal nucleation and growth kinetics [12], using membrane distillation, also known as pervaporation. This process is known as membrane crystallisation, with proven applications for crystallising LiCl [13], NaCl [14,15], Na_2CO_3 [16] and $MgSO_4$ [17]. Owing to the fast pervaporation of solvent via the hydrophobic polymeric membrane, ideal conditions are created at surface of the membrane at the feed side, leading to supersaturation, nucleation and crystallisation. Subsequently, two further downstream processes are required where (i) crystals are separated from the solution by filters and then (ii) dried in furnaces.

Although the state of the art in polymeric membrane crystallisation is well known, inorganic ceramic membranes remained absent [18] in this technological development until recently by the pioneering work of Motuzas and co-workers [19] who prepared porous hydrophobic carbon membranes to crystallise NaCl from mineral brine solutions. This process is known as membrane percrystallisation as solutes (i.e., crystals) and solvents were separated at a single step by a wet thin film under vacuum on the permeate side of the membrane. Subsequently, it was demonstrated that the process conditions (i.e., flow rates, temperature and vacuum pressure) in membrane percrystallisation altered the crystal NaCl particle size [20], and the crystal phase of $NiSO_4$ [21]. The use of hydrophilic inorganic membranes has eluded the field of membrane crystallisation to date.

Therefore, this work demonstrates for the first time that hydrophilic inorganic membranes can be used efficiently for crystallising mineral brines by a novel pore storage mechanism under pervaporation. It is shown that salt storage in the macropores of a ceramic membrane substrate under pervaporation can be attained only in the presence of a mesoporous inorganic top-layer with controlled pore sizes. Further, this work demonstrates that fundamental mass transfer properties in the pore storage are a function of feed concentrations for a single salt, and as a function of the molecular weight for chloride salts.

2. Experimental

2.1. Sol-gel synthesis and xerogel characterisation

An aqueous aluminium oxide (20%) sol with an average colloidal particle size of 0.05 μm (pseudo-boehmite from Alfa Aesar) was used as received for coating gamma alumina interlayers. The top layers were synthesised using a titania sol-gel method. Briefly, titanium (IV) isopropoxide (TIP, $TiC_{12}H_{28}O_4$, 98%, Sigma-Aldrich) was added drop-wise into a solution of double-distilled water and hydrochloric acid under vigorous stirring. Then the mixture was maintained in a water bath at 30 °C for 3 h. The molar ratio of the final sol was TIP:HCl:H_2O = 1:1:22. The sol was then dried in an oven at 60 °C for 3 h.

The preparation of xerogel (dried gel) was initially carried out by heat treatment at 150 °C to ensure the consolidation of the titania matrix. Subsequently, the titania xerogel was calcined at 350 °C to condense the matrix into a meso-structure. Heat treatment and calcination were carried out at a heating/cooling rate of 1 °C min^{-1} and a dwell time of 1 h. Nitrogen sorption of titania xerogel samples was conducted on a Micromeritics TriStar 3020 analyser after degassing under vacuum on a Micromeritics VacPrep061 at 200 °C for a minimum of 12 h. The specific surface areas were calculated from the adsorption isotherms via the multi-points BET model at relative pressures of p/p_o = 0.05–0.3. The pore size distribution was determined using Barrett–Joyner–Halenda (BJH) model, from the desorption branch of the isotherms of the mesoporous titania xerogel samples.

2.2. Membrane preparation and characterisation

Commercial porous alpha alumina (α-Al_2O_3) tubes (OD = 1 cm, ID = 0.5 cm, L = 5.5 cm, Ceramic Oxide Fabricator Pty Ltd.) were used as membrane substrates. The substrates were pre-calcined at 1000 °C for 8 h with a ramp rate of 5 °C min^{-1} to improve the mechanical strength and to remove any organic impurities. Each coated layer was deposited separately by a dip-coating method at immersion and withdrawal rate of 5 cm min^{-1} and a dwell time of 1 min. Both ends of the substrate were closed prior to dip-coating to allow layers to be coated on the outer shell of the substrate only. After each coated layer, the membranes were calcined in air at 500 °C (gamma alumina interlayers), 150 and 350 °C (titania top layers) at a ramping/cooling rate of 1 °C min^{-1} and a dwell time of 1 h. The latter followed a procedure proposed by Yacou et al. [22] in order to control the mesopore size of titania thin films. The final prepared membranes consisted of two gamma alumina interlayers and two titania top layers. Microstructural investigation of the membrane layers was carried out via a JEOL field emission scanning electron microscope (FE-SEM, JEOL JSM-7001F) operating at 5 kV at a working distance of 10 mm.

2.3. Membrane crystallisation

Synthetic feed solutions were prepared by mixing chloride based salts (mol_s) with the required amount of double-distilled water (L_w) represented by $mol_s\ L_w^{-1}$. The salt concentration of the feed solution was determined via standard calibration curves (conductivity versus concentration) using a conductivity meter (labCHEM CP). The membrane outer shell was exposed to a pre-determined salty feed solution at atmospheric pressure and room temperature (~20 °C). The inner shell of the membrane (i.e., permeate side) was evacuated to 18 mbar using a vacuum pump, thus allowing water to evaporate and salt to remain in the pores of the membrane. The effective length of the membrane for pervaporation testing was 4.5 cm, as 0.5 cm at both ends of the substrate were covered with silicon tubes. The membranes were tested at time intervals from 10 to 30 min. The water vapour in the permeate stream was condensed and collected in a liquid nitrogen cold trap located downstream. The collected water was analysed using the conductivity meter to determine if any salt ions were entrained in the water vapour during water evaporation.

After testing, the membranes were transferred to a pre-heated oven at 60 °C for 8 h to ensure a complete crystallisation of salts on the TiO_2 top layer took place on the outer shell of the membrane. The pervaporation schematic and salt growth on the membrane surface is depicted in the Appendix Fig. A1. The relative humidity of the oven chamber (RH = 67.3%) was controlled using $NaNO_3$ brine solution. Salt crystals on the surface of the membranes were observed with JEOL field emission scanning electron microscope (FE-SEM, JEOL JSM-7001F) operating at 5 kV at a working distance of 10 mm.

The crystallised salts were removed from the outer surface of the membrane and the collected mass of salt crystals was measured in a high-precision laboratory scale. This allowed the production (***J***) of crystallised salts to be determined as follows,

$$J = \frac{m_{salt}}{tA} \tag{1}$$

where $\boldsymbol{m_{salt}}$ is the mass of crystallised salt collected at a pre-determined membrane pervaporation time interval $\boldsymbol{t}$ (min), and $\boldsymbol{A}$ (m^2) is membrane surface area. The membrane pervaporation followed by oven drying were replicated at least five times for all tested conditions. A Panasonic microwave (Genius 1100 MW) with variable power was also used for drying and crystallising chloride base salts. The membranes were microwave-dried at 900 W for 2 min. The mass and flux of crystallised chloride base salts after microwave-dried were calculated using a similar procedure as described above for the oven-dried membranes.

3. Results and discussion

3.1. Induced crystallisation and membrane characteristics

Here we demonstrate for the first time that hydrophilic inorganic ceramic membranes are very efficient in processing mineral brines by a

novel mechanism of induced salt crystallisation. We observed that under pervaporation of an aqueous NaCl solution, salts concentrated in the pores whilst water permeated through the membrane. Upon drying the membrane, capillary forces in the pores induced evaporation of water, leading to super-saturation, nucleation and crystal growth on the surface of the membrane. Fig. 1 displays NaCl crystals grown perpendicular to the membrane surface which appear as a salt crystal forest-type arrangement. The crystals are unusual, having a cubic shaped base at the interface of the membrane followed by an elongated pyramid shape, in sharp contrast to conventional NaCl cubic crystals. It is noteworthy that the crystals are approximately equidistant from each other.

Analysis of the SEM image (Fig. 1) suggests that the base of the crystal is of ~20.5 (±2) μm, and the average distance between each crystal base is ~15.1 (±1.5) μm. Therefore, one square metre of inorganic membrane area generates on the order of 789 million nucleation points of these unusual crystals in a single processing cycle of pervaporation, pore storage and crystallisation. As salt ions are expelled from the pores of the membrane, their concentration increases on the surface of the membrane. This process of mass transfer leads to spontaneous crystal nucleation in a supersaturated thin wet film on the surface of the membrane. Upon formation of the stable nuclei, crystal growth predominates which lowers the local supersaturation and inhibits further nucleation. Consequently, salt ions diffuse on the surface of the membrane from areas of high concentration to low concentration due to the chemical potential, thus favouring crystal growth.

Induced salt crystallisation occurred in asymmetric membranes (see representative SEM image in Fig. 2) composed of two top layers (titania) and two interlayers (gamma-alumina) with a combined average thickness of 1.95 μm coated on an alpha-alumina support. The asymmetric configuration is based on the principle that the thin top layers are coated on a mechanically strong substrate, whilst the interlayer provides a smooth surface to form a defect free thin top layer [23]. A fundamental aspect of this induced pore crystallisation is the precise control of the sol-gel method to tailor the inorganic hydrophilic membrane pore diameter (d_p). This was achieved by an acid sol-gel synthesis of the titania top layers followed by a two-step calcination to 150 and 350 °C and using a low ramping rate of 1 °C min^{-1}. A number of hydrophilic membranes were tested under pervaporation of aqueous NaCl solutions. The pore size of macroporous alpha alumina (d_p > 50 nm) were too large, resulting in pore wetting and full permeation of the solution. In the case of microporous silica membranes (d_p < 0.5 nm or 5 Å) [24], only water diffused through the membranes as the permeation of salt ions were hindered. Pore storage was observed for mesoporous titania top-layers (3 < dp < 5 nm) (Fig. 2 inset) and gamma alumina (3.7 < dp < 8.9 nm) [25] interlayers.

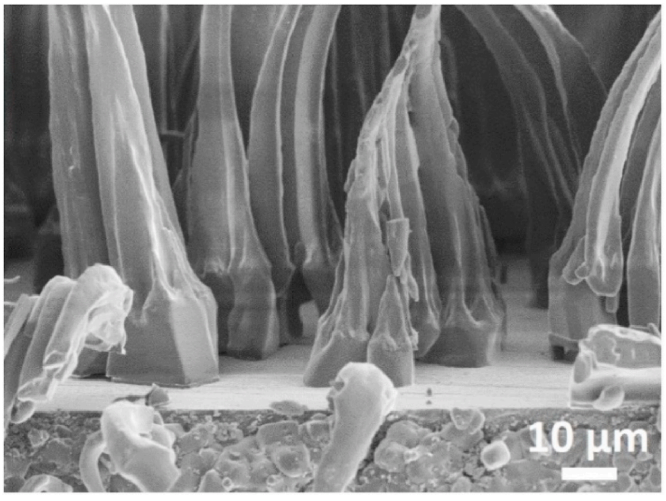

Fig. 1. SEM image of NaCl crystal pyramid-like shapes on a membrane dried at 60 °C.

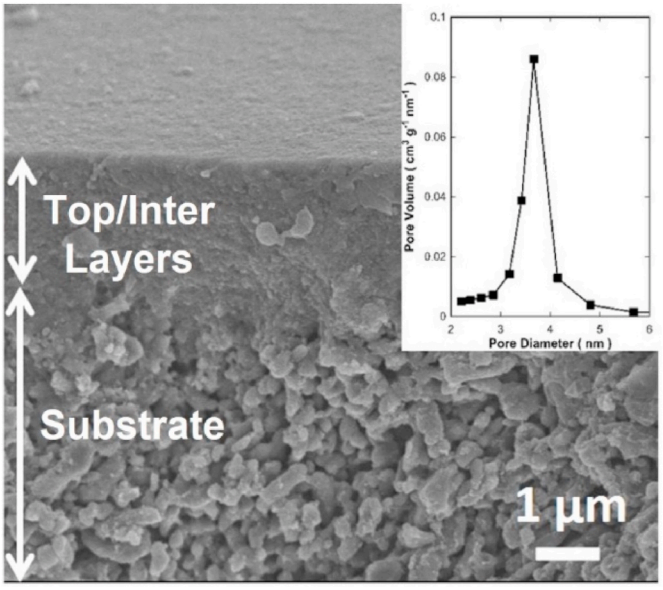

Fig. 2. SEM image of an asymmetric titania (top-layer) and gamma alumina (interlayer) where inset shows a pore size distribution based on Barrett, Joyner and Halenda (BJH) model.

3.2. Membrane performance

Fig. 3 shows the stable cyclic performance of the titania/alumina membrane over 10 consecutive cycles of pervaporation and NaCl crystallisation. Increasing the NaCl feed concentration resulted in an increase in the production of NaCl crystals, suggesting an increase in the storage rate of NaCl in the pores of the membranes. Notably, the titania/alumina membrane was able to process a wide range of feed solution concentrations ranging from seawater (0.6 mol L_w^{-1} NaCl) to hypersaline brines (5.4 mol L_w^{-1} NaCl).

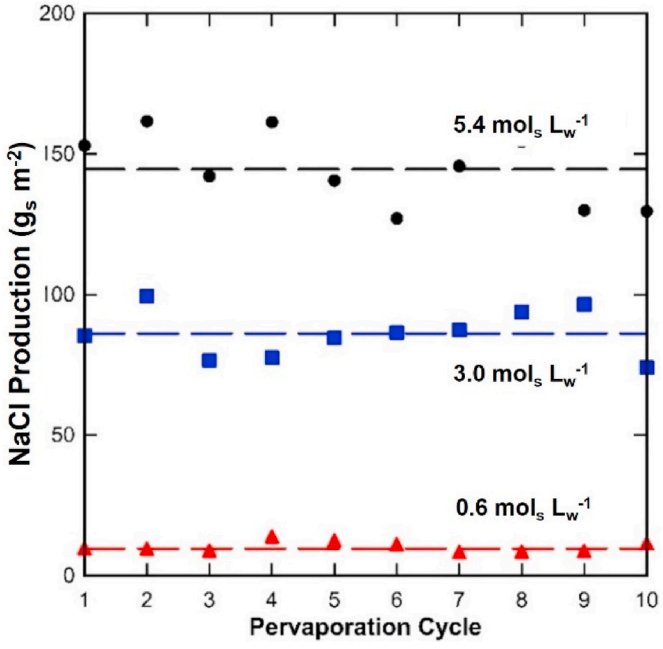

Fig. 3. NaCl production rate for 10 successive cycles of pervaporation of 30 min for various NaCl feed concentrations (0.6, 3.0 and 5.4 mol L_w^{-1}). The membranes were oven-dried at 60 °C for 8 h and RH = 67.3%.

This novel induced crystallisation proved to be very effective for a number of chloride salts as displayed in Fig. 4. Under cycles of pervaporation of 10 min, the salt storage in the nanopores varied between 50 and 63 g m^{-2}, except for LiCl. It was observed that Li had reacted slightly with the membrane as the top layer became darker instead of the typical white titania colour. The Li reaction along with the relatively low molar mass of Li explains the lower LiCl storage per cycle.

3.3. Novel pore storage mechanism

Salt crystallisation on the membrane surface proceeded via pervaporation as schematically depicted in Fig. 5. Upon contact of the dry membrane with an aqueous salt solution, capillary forces take effect immediately [26]. These forces induced salt solution penetration into the pores due to the hydrophilic nature of titania and gamma-alumina layers. Based on the results in Fig. 3 for a feed solution of 5.4 mol L_w^{-1}, the NaCl production average is 144.5 g m^{-2}. This is equivalent to a NaCl crust of NaCl with a thickness of 67 μm. The latter is 35 times thicker than the average thickness of the mesoporous titania and gamma-alumina layers of 1.95 μm. Therefore, the mass of salt that causes induced crystallisation can be directly attributed to salt storage in the membrane substrate that accounts to 99.96% of the overall membrane thickness. Theoretical calculations in the Appendix Table A1 clearly confirms that this is the case as there is sufficient pore volume in the membrane substrate to accommodate the NaCl mass that induced crystallisation.

It is noteworthy the role played by the mesoporous titania and gamma-alumina layers in avoiding membrane flooding under pervaporation. In this case, the mesoporous layers modulated the flow of salt ion solution into the larger macropores of the substrate. This flow modulation benefited the salt storage mechanism by entraining salt ions in the macropores of the substrate whilst avoiding solution flooding in the permeate side.

In this process, menisci are formed in the macropores of the substrate close to the surface of the inner shell of the tubes under pervaporation, thus controlling the water evaporation via the permeate stream. The water evaporation at the menisci is controlled by vapour-liquid equilibrium according to the Kelvin equation [27]. The water pervaporated through the membrane was condensed in a liquid nitrogen cold trap and analyses indicated salt rejections in excess of 99%, confirming that salt ion solution was mainly retained in the macropores of the substrate of the membrane.

Upon drying the membrane, induced salt crystallisation on the surface of the mesoporous titania top layer took place. This process is directly controlled by capillary forces. As the macropores of the alpha-alumina substrate are interconnected to the mesopores of gamma-alumina interlayers and that to the mesopores of the titania layer, capillary pressure gradients force the salt ion solution stored in the substrate to permeate from the macropores to the mesopores. This is the case for two different saturated porous materials in hydraulic contact with each other and dried, the material with the largest pores starts to drain first [28]. Upon drying further, capillary forces bring the salt ion solution to the surface of the titania top layer where water evaporation increases rapidly. As a result, salt ions on the membrane surface reach supersaturation and lead to salt nucleation and salt growth induction as evidenced by Fig. 1.

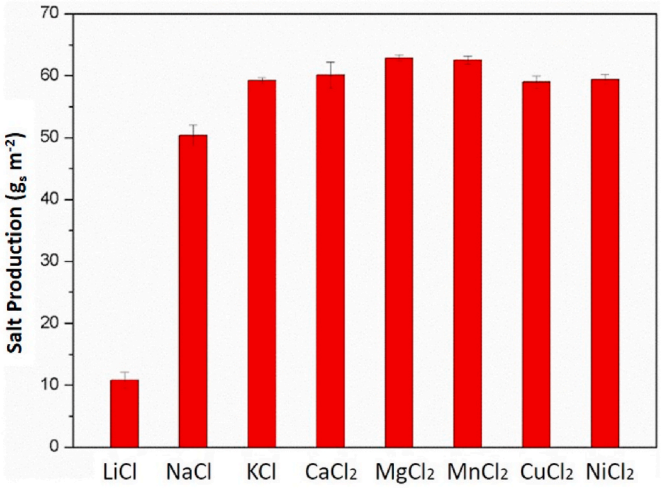

Fig. 4. Chloride salt production for feed concentrations (3 mol_s L_w^{-1}) at 20 °C with a pervaporation time of 10 min. The membranes were microwave-dried at 900W for 2 min. Salt production includes hydrated salts.

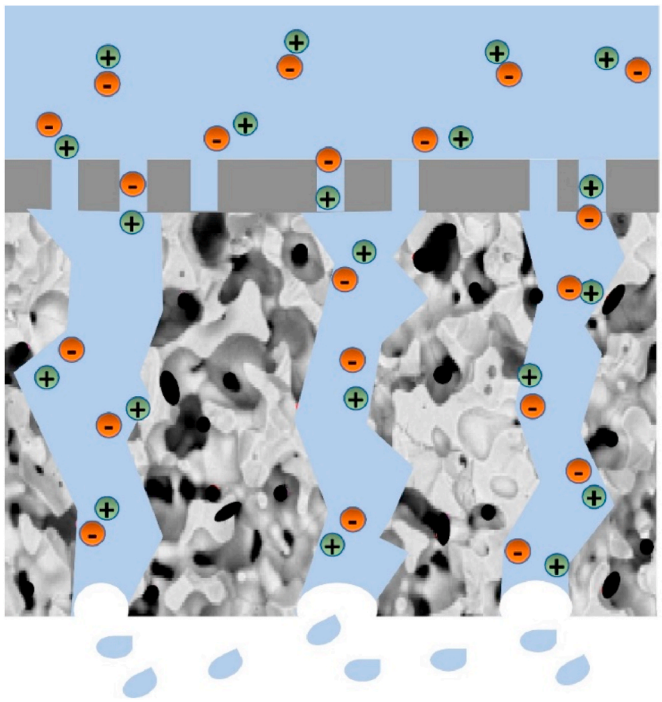

Fig. 5. Idealised schematic representing the salt storage in the membrane where is the salt feed solution, is the titania and gamma alumina mesoporous layers, is the water meniscus, is water vapour and is the alpha alumina macroporous substrate.

3.4. Transport phenomena, salt production and storage coefficients

During the pervaporation stage, salt is being concentrated in the membrane pores (c_p) as the process is driven by vacuum evaporation of water. A concentration gradient (Δc) is thus established between the solution in the membrane pores and the solution in the feed. Fig. 6 shows the continuous built up of NaCl in the membrane pores as a function of time until a maximum salt storage capacity is reached. At this maximum capacity, the pores are fully saturated with salt solution and equilibrium is achieved between the salt concentration in the feed solution and that in the macropores. In addition, the salt production capacity also increased as a function of the NaCl feed concentration. Hence, the transport phenomenon in this membrane pore storage mechanism is associated with the salt concentration in the feed solution. The driving force for salt storage is at the highest at the beginning of pervaporation ($t = 0$) and minimum at the maximum storage or saturation time ($t = t_{sat}$). In other words, the membrane pore storage mechanism is characterised by a batch process of salt loading.

Interestingly, the production of NaCl as a function of the feed concentration fitted well to a linear relationship (R^2>0.99) as demonstrated

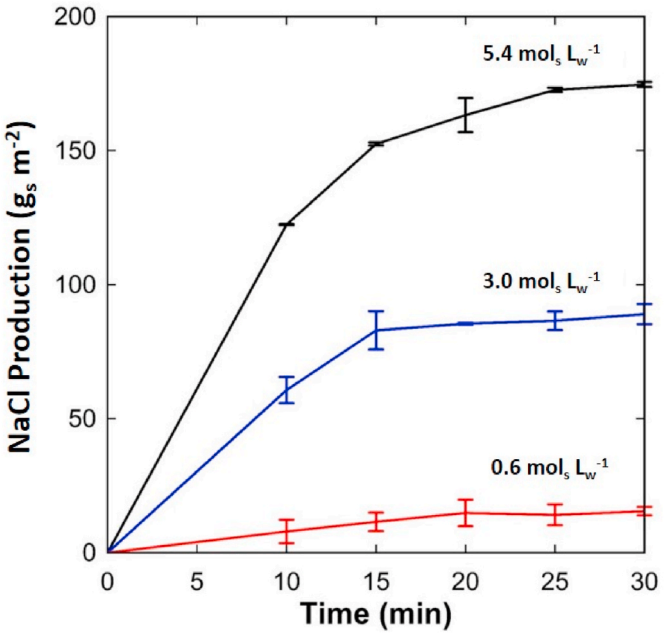

Fig. 6. NaCl production as a function of pervaporation time for a porous membrane tube thickness of 2.5 mm for various NaCl feed concentration (0.6, 3.0 and 5.4 mol L_w^{-1}). The membranes were oven dried at 60 °C for 8 h and RH = 67.3%.

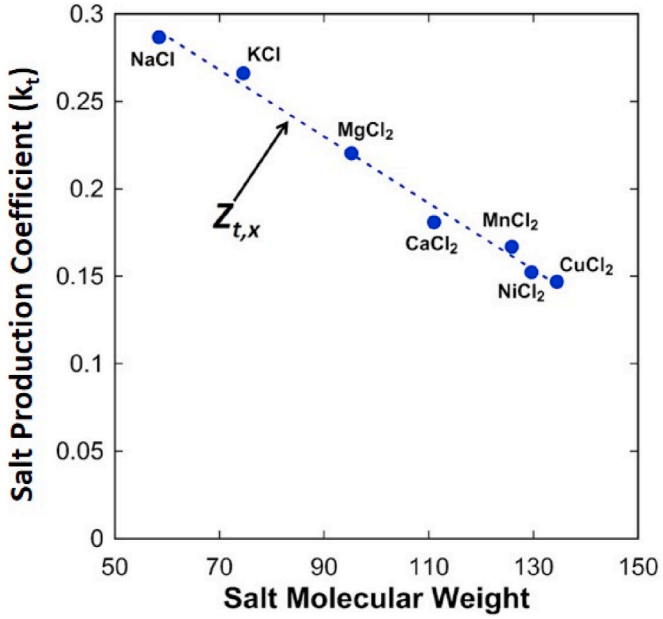

Fig. 8. Global salt production coefficient ($Z_{t,x}$) for a series of non-reactive chloride base salts (3 mol L^{-1} feed solutions at 20 °C) for a pervaporation time of 10 min and microwave drying at 900 W and 2 min. Salt production coefficient includes hydrated salts.

in Fig. 7a. We define the slope of this linear relationship as a salt production coefficient (k_t), which provides a fundamental parameter of this novel membrane pore storage process. Owing to the batch process characteristics, the salt production coefficients were plotted against time as shown in Fig. 7b, using data from Fig. A2 in the Appendix where all R^2>0.99. After 20 min, NaCl accumulation in the pores reached saturation level (k_{sat}), suggesting an approach to equilibrium when the driving force is no longer significant. These results clearly indicate that the mass storage mechanism in the membrane pores of the hydrophilic inorganic membrane follows Eq. (1) for a given condition, where $\boldsymbol{P}$ is the membrane surface area specific salt production (mol$_s$ m^{-2}), $\boldsymbol{t}$ is the pervaporation time, $\boldsymbol{k}$ is the salt production coefficient (mol$_s$ L$_w$ mol$_s^{-1}$ m^{-2}) and $\boldsymbol{c_f}$ is the feed salt concentration (mol$_s$ L$_w^{-1}$).

$$P_t = k_t c_f \tag{2}$$

Another fundamental parameter for this novel pore storage mechanism is termed the global salt production coefficient ($\boldsymbol{Z}$). The $\boldsymbol{k_t}$ values of the chloride salts in Fig. 8 derived from Fig. 4 were plotted against their molecular weights, excluding LiCl which slightly reacted with the membrane to some extent. Remarkably, the slope (Z) shows a linear relation (also R^2>0.99), clearly indicating that salt production is also a function of the molecular weight of the non-reactive chloride salts tested in this work. Therefore, Eq. (2) describes this property, where $\boldsymbol{t}$ is the pervaporation time, $\boldsymbol{k}$ is the salt production coefficient and $\boldsymbol{m}$ is the molecular mass of salt $\boldsymbol{x}$. The slope $\boldsymbol{Z = -317m_x+187}$ for the chloride salts tested in this work.

$$k_{t,x} = Z_{t,x} m_x \tag{3}$$

Essentially salt solutions were stored in the membrane during pervaporation, so the pore storage coefficients are volumetric as a function of the membrane surface area and membrane thickness. Hence, the mass storage coefficient ($\boldsymbol{S_t}$), Eq. (4), is the mass of salt mainly stored in the macropores of the substrate (mol$_s$ m^{-2} m^{-1}), per area (m^2) per membrane thickness $\boldsymbol{l}$ (m), which can be derived from Eq. (2) as follows:

$$S_t = \frac{P_t}{l} \tag{4}$$

Likewise, the global salt storage coefficient $\boldsymbol{GS_{t,x}}$, Eq. (5), for a membrane thickness $\boldsymbol{l}$ (m) can be derived from Eq. (3). As the slopes of

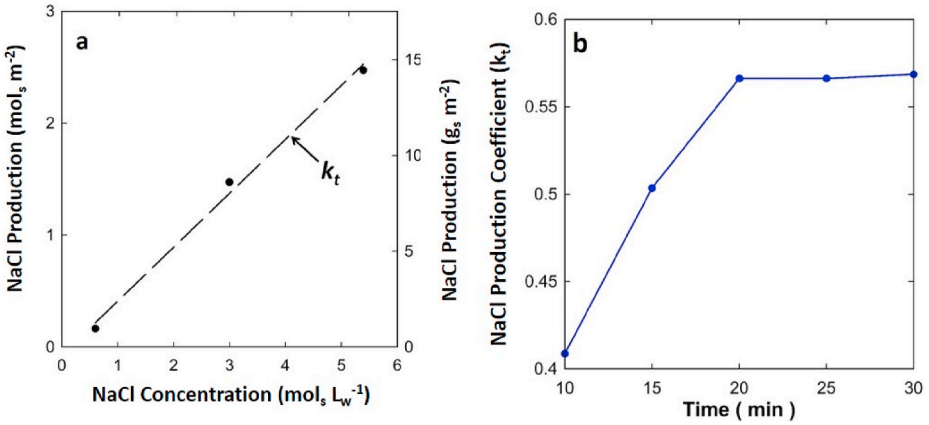

Fig. 7. (a) NaCl production versus feed concentration at 30 min pervaporation time, and (b) NaCl production coefficient (k_t) versus time.

$\boldsymbol{Z_{t,x}}$ and $\boldsymbol{GS_{t,x}}$ remain the same irrespective of the thickness of the membrane, than both global salt production and global salt storage coefficients for chloride hydrates are the same as follows:

$$GS_{t,x} = Z_{t,x} \quad (5)$$

In principle, the capability of the membrane to store salt is a function of the membrane specific structure. Hence, salt production values increase by increasing the thickness of the substrate, or by increasing the porosity of the substrate provided that membrane flooding is avoided. However, if increased in salt production are proportional to the feed concentration and/or to the chloride salt tested, then the slopes may remain the same. This means that the coefficients k_t and Z_t may not be affected by the membrane's specific structure if salt production proportionality is maintained.

4. Conclusions

The induced crystallisation of mineral brines using hydrophilic inorganic membranes occurred via a novel mechanism of membrane pore salt storage during pervaporation. This phenomenon occurred due to the modulation of salt ion solution via the mesopores of titania and gamma-alumina layers, thus avoiding pore flooding in the substrate macropores. Fundamental properties of the membrane pore mass storage were established by determining salt production coefficient for single salts, and a global salt storage coefficient as a function of the molecular weight of chloride salts. These coefficients form the basis for the design of industrial plants for processing brines.

Declaration of competing interest

The authors declare that they have no known competing financial interests or personal relationships that could have appeared to influence the work reported in this paper.

Acknowledgement

The authors acknowledge the financial support from the Australian Research Council (DP1901002502) and (DP190101734) grants. J. C. Diniz da Costa gratefully thanks the support given by the French "Centre National de la Recherche Scientifique" (CNRS-INC section 15) grant as invited Professor at the Institut Européen des Membranes de Montpellier in France, and the Visiting Fellowship d by the Associate Laboratory for Green Chemistry – LAQV, financed by the Portuguese National Government funds from FCT/MCTES (UIDB/50006/2020).

Appendix

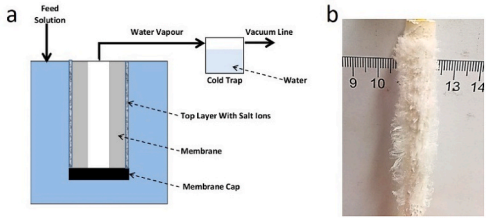

Fig. A1. (a) Schematic of the pervaporation process and (b) image of an oven-dried membrane.

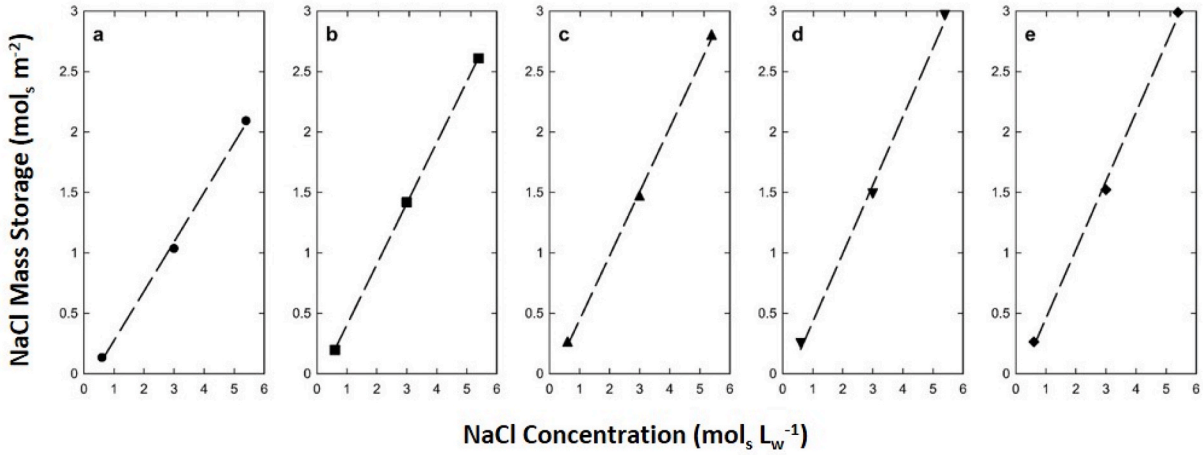

Fig. A2. Mass storage (average values) versus NaCl concentration for a series of pervaporation times: (a) 10 min, (b) 15 min, (c) 20 min, (d) 25 min and (e) 30 min where all R^2>0.99.

The alpha-alumina substrate porosity of 36% was determined from helium pycnometry. The substrate's pore volume ($\boldsymbol{p_{vol}}$) is 675 mL for a membrane tube with a surface area of 1 m^2, 1 cm outer shell diameter and a wall thickness of 2.5 mm. Table A1 lists the average density ($\boldsymbol{\rho}$) for the NaCl feed concentrations used in this work. The NaCl densities were determined based soaking conditions of a a membrane with 1 m^2 surface area with a solution in equilibrium with the feed temperature. The mass of salt ($\boldsymbol{M}$) stored in the pores of the membrane is determined by $M = \rho\, p_{vol}$. Table A1 shows the NaCl mass stored mainly in the macropores of the substrates which are 99.96% of the total porosity. The NaCl production results from Fig. 3 are also listed. These results show that theoretical mass of NaCl stored in the substrate is always higher than the mass produced per 1 m^2 of membrane surface area.

Table A1
Theoretical NaCl mass stored in the membrane pores for a membrane with 1 m ^{2} of surface area and pore volume of 675 mL.

Sol conc.	Sol conc.	Av. density	Membrane Mass sol	Membrane NaCl mass	Fig. 3 results NaCl mass
($mol_s\ L_w^{-1}$)	Wt%	($g\ L^{-1}$)	(g_{sol})	(g_s)	(g_s)
0.6	3.4	1022.3	690.4	23.5	16.2
3	14.9	1107.8	748.2	111.5	88.9
5.4	24	1180.4	797.2	191.3	174.0

References

[1] Z. Fang, J. Wang, H. Wu, Q. Li, S. Fan, J. Wang, Progress and challenges of flexible lithium ion batteries, J. Power Sources 454 (2020) 227932.
[2] T. Nemeth, P. Schröer, M. Kuipers, D.U. Sauer, Lithium titanate oxide battery cells for high-power automotive applications – electro-thermal properties, aging behavior and cost considerations, J. Energy Storage 31 (2020) 101656.
[3] M. Arbabzadeh, R. Sioshansi, J.X. Johnson, G.A. Keoleian, The role of energy storage in deep decarbonization of electricity production, Nat. Commun. 10 (2019) 3413.
[4] S.E. Kesler, P.W. Gruber, P.A. Medina, G.A. Keoleian, M.P. Everson, T. J. Wallington, Global lithium resources: relative importance of pegmatite, brine and other deposits, Ore Geol. Rev. 48 (2012) 55–69.
[5] U. Bardi, Extracting minerals from seawater: an energy analysis, Sustainability 2 (2010) 980–992.
[6] U. Grober, J. Schmidt, K. Kisters, Magnesium in prevention and therapy, Nutrients 7 (2015) 8199–8226.
[7] S. Mahamuni, A.D. Lad, S. Patole, Photoluminescence properties of manganese-doped zinc selenide quantum dots, J. Phys. Chem. C 112 (2008) 2271–2277.
[8] C. Favero, M.B. Closs, G.B. Galland, R. Stieler, E. Rossetto, K. Bernardo-Gusmão, A binary nickel diimine-MCM-41 supported catalyst and its application in ethylene polymerization, J. Catal. 377 (2019) 63–71.
[9] C. Zörb, M. Senbayram, E. Peiter, Potassium in agriculture – status and perspectives, J. Plant Physiol. 171 (2014) 656–669.
[10] S. Pacala, R. Socolow, Stabilization wedges: solving the climate problem for the next 50 years with current technologies, Science 305 (2004) 968–972.
[11] D.S. Sholl, R.P. Lively, Seven chemical separations to change the world, Nature 532 (2016) 435–437.
[12] E. Drioli, G. di Profio, E. Cursio, Progress in membrane crystallisation, Curr. Opin. Chem. Eng. 1 (2012) 178–182.
[13] C.A. Quist-Jensen, A. Ali, S. Mondal, F. Macedonio, E. Drioli, A study of membrane distillation and crystallization for lithium recovery from high-concentrated aqueous solutions, J. Membr. Sci. 505 (2016) 167–173.
[14] X. Ji, E. Curcio, S. Al Obaidani, G. Di Profio, E. Fontananova, E. Drioli, Membrane distillation-crystallization of seawater reverse osmosis brines, Separ. Purif. Technol. 71 (2010) 76–82.
[15] G. Chen, Y. Lu, W.B. Krantz, R. Wanga, A.G. Fane, Optimization of operating conditions for a continuous membrane distillation crystallization process with zero salty water discharge, J. Membr. Sci. 450 (2014) 1–11.
[16] W. Ye, J. Lin, Shen, P. Luis, B. Van der Bruggen, Membrane crystallization of sodium carbonate for carbon dioxide recovery: effect of impurities on the crystal morphology, Cryst. Growth Des. 13 (2013) 2362–2372.
[17] L. Mariah, C.A. Buckley, C.J. Brouckaert, E. Curcio, E. Drioli, D. Jaganyi, D. Ramjugernath, Membrane distillation of concentrated brines - role of water activities in the evaluation of driving force, J. Membr. Sci. 280 (2006) 937–947.
[18] E. Chabanon, D. Mangin, C. Charcosset, Membranes and crystallization processes: state of the art and prospects, J. Membr. Sci. 509 (2016) 57–67.
[19] J. Motuzas, C. Yacou, R.S.K. Madsen, W. Fu, D.K. Wang, A. Julbe, J. Vaughan, J. C. Diniz da Costa, Novel inorganic membrane for the percrystallization of mineral, food and pharmaceutical compounds, J. Membr. Sci. 550 (2018) 407–415.
[20] R.S.K. Madsen, J. Motuzas, A. Julbe, J.C. Diniz da Costa, Fine control of NaCl crystal size and particle size in percrystallisation by tuning the morphology of carbonised sucrose membranes, J. Membr. Sci. 567 (2018) 157–165.
[21] R.S.K. Madsen, J. Motuzas, A. Julbe, J. Vaughan, J.C. Diniz da Costa, Novel membrane percrystallisation process for nickel sulphate production, Hydrometallurgy 185 (2019) 210–217.
[22] C. Yacou, S. Smart, J.C. Diniz da Costa, Mesoporous TiO_2 based membranes for water desalination and brine processing, Separ. Purif. Technol. 147 (2015) 166–171.
[23] A.F.M. Lenaars, A.J. Burggraaf, The preparation and characterisation of alumina membranes with ultrafine pores. Part 2 - the formation of supported membranes, J. Colloid Interface Sci. 105 (1985) 27–40.
[24] C.X.C. Lin, L. Ding, Simon K. Smart, J.C. Diniz da Costa, Cobalt oxide silica membranes for desalination, J. Colloid Interface Sci. 368 (2012) 70–76.
[25] A.F.M. Lenaars, K. Keizer, A.J. Bruggraaf, The preparation and characterisation of alumina membranes with ultrafine pores. Part 1 - microstructural investigation on non-supported membranes, J. Mater. Sci. 19 (1984) 1077–1088.
[26] K.G. Kornev, A.V. Neimark, Spontaneous penetration of liquids into capillaries and porous membranes revisited, J. Colloid Interface Sci. 235 (2001) 101–113.
[27] K.W. Lawson, D.R. Lloyd, Membrane distillation, J. Membr. Sci. 124 (1997) 1–25.
[28] V. Voronina, L. Pel, A. Sawdy, K. Kopinga, The influence of osmotic pressure on poulticing treatments for cultural heritage objects, Mater. Struct. 46 (2013) 221–231.